

The effect of charm quark on the QCD chiral phase diagram

Fei Gao ¹, Yuepeng Guan ² and Shinya Matsuzaki ²

¹*School of Physics, Beijing Institute of Technology, 100081 Beijing, China*

²*Center for Theoretical Physics and College of Physics, Jilin University, Changchun, 130012, China*

We study the influence of charm quark dynamics on the chiral phase structure of Quantum Chromodynamics (QCD) using the recently developed miniDSE scheme of the Dyson–Schwinger equations. By calculating the quark propagator in $2+1$ and $2+1+1$ flavor QCD, we quantify the impact of including the charm quark as a dynamical degree of freedom on the QCD phase diagram. Our results show that the charm quark induces a moderate but noticeable shift to lower chemical potential in the location of the critical endpoint (CEP) by approximately 2–3%. The result in this work indicates that the heavy-flavor dynamics can subtly influence the QCD phase structure and should be taken into account in particular for searching the CEP of QCD.

I. INTRODUCTION

Quantum Chromodynamics (QCD), the fundamental theory governing the strong interaction, exhibits a rich and intricate phase structure. The most intriguing feature there is the spontaneous breaking and the restoration of chiral symmetry, which underlies the dynamical generation of baryon masses. A detailed understanding of the chiral phase transition is not only essential for deciphering the nonperturbative dynamics of QCD but also has profound implications for a wide range of physical phenomena, including the physics of heavy-ion collisions [1–5], the equation of state of neutron stars [6–8], and the thermal evolution of the early universe [9–12].

Over the past decades, considerable efforts have been devoted to exploring the QCD chiral phase structure, particularly in systems with two or two-plus-one quark flavors. These investigations span a variety of nonperturbative techniques, including effective models and extrapolation methods [13–24], and first principle QCD approaches like lattice QCD simulation [25–27], functional QCD (fQCD) methods including the Dyson–Schwinger equations (DSEs) [28–34] and functional Renormalization Group (fRG) approach [35–37]. These studies have converged on a picture in which, at vanishing baryon density, the chiral transition for light quarks is a smooth crossover occurring at a pseudo-critical temperature of approximately $T_c \sim 150$ MeV. At finite density, evidence points toward the existence of a critical endpoint (CEP) at a baryon chemical potential around $\mu_B^{\text{CEP}} \sim 600$ MeV. The prediction for the CEP location is particularly important as it may shed light on the precision measurement in the heavy ion collision experiments [5, 38].

Most of the theoretical calculations on QCD phase transitions, however, neglect the contribution of heavy quark flavors, particularly charm and bottom, based on the decoupling theorem, which asserts that heavy flavors should have little influence on the infrared (IR) dynamics of QCD. Nevertheless, the heavy quark dynamics including the charm fluctuations, the heavy quark drag and diffusion coefficients are important for the related phenomena in heavy ion collisions [39, 40]. In the pioneering works within a simplified truncation scheme of DSEs, it

is found that the CEP location is barely changed with the inclusion of the charm quark loop [29, 41].

The present work revisits the influence of charm quark dynamics on the QCD chiral phase structure using the recently proposed miniDSE approach [42]. This framework offers a numerically efficient and systematically improvable formulation of the Dyson–Schwinger equations, allowing for the seamless inclusion of additional quark flavors with controlled approximations and quantified uncertainties. Within this setting, we compute and compare the chiral phase diagrams of QCD with and without the charm quark. Our results reveal that the presence of the charm flavor induces a noticeable shift in both the location of the CEP and the shape of the crossover boundary, thereby underscoring the potential significance of heavy-flavor effects in QCD phase structure studies.

This paper is arranged as follows. In Sec. II, we briefly introduce the quark and gluon propagator DSEs of QCD and summarize the truncation scheme in the current work. In Sec. III, we show the impacts of the charm quark loop on the physical observables in vacuum. Then, we present the chiral phase diagram obtained from the different cases, and list the observed quantities from the phase diagrams. The conclusions and discussions are put in Sec. IV.

II. DYSON-SCHWINGER EQUATIONS AT FINITE TEMPERATURE AND CHEMICAL POTENTIAL

In the current work, we employ the computationally minimal truncation scheme for the DSE approach (miniDSE) of QCD provided in Ref. [42]. The strategy is to solve the quark gap equations self-consistently, and deal with the difference of DSE for the gluon propagator with respect to the input data coming from other quantitative approaches. The coupled equation would be closed after we impose the dressing functions for the quark-gluon vertices with leading-order tensorial structures, i.e., the Dirac and Pauli terms.

We formulate the DSEs in the Landau gauge and pa-

parameterize the quark and gluon propagators as

$$\begin{aligned} [S^f(\tilde{p})]^{-1} &= i\tilde{\omega}_n^\psi \gamma_4 C^f(\tilde{p}) + i\mathbf{p} \cdot \boldsymbol{\gamma} A^f(\tilde{p}) + B^f(\tilde{p}), \\ D_{\mu\nu}(k) &= G_A(k) \Pi_{\mu\nu}^\perp, \end{aligned} \quad (1)$$

where the flavor index takes $f = u, d, s, c$. In Eq. (1), the scalar part of the gluon propagator reads

$$G_A(k) = \frac{Z_A(k)}{k^2}. \quad (2)$$

We adopt the $O(4)$ -symmetric approximation for the gluon propagator such that the chromoelectric and the chromomagnetic parts do not split from each other. The momentum arguments of quarks and gluon are given by $\tilde{p}_\mu = (\tilde{\omega}_n^\psi, \mathbf{p})$ and $k = (\omega_n^A, \mathbf{k})$, with $\tilde{\omega}_n^\psi = \omega_n^\psi + i\mu_q = (2n+1)\pi T$ and $\omega_n^A = 2n\pi T$. The quark chemical potential takes $\mu_q = \mu_B/3$ with the flavor-universal baryon chemical potential μ_B .

A. The quark gap equation

The quark gap equations for each flavor read

$$[S^f(\tilde{p})]^{-1} = [S_0^f(\tilde{p})]^{-1} + \Sigma_0^f(\tilde{p}), \quad (3)$$

where the expression of quark self-energy Σ_0^f is given by

$$\Sigma_0^f(\tilde{p}) = \frac{4}{3} Z_1^f g_s \int_q \gamma_\mu S^f(\tilde{q}) \Gamma_\nu^f(\tilde{q}, \tilde{p}) D_{\mu\nu}(k), \quad (4)$$

where $k_\mu = \tilde{q} - \tilde{p}$, with the shorthand notation $\int_q = T \sum_n \int d^3\mathbf{k}$. Following the miniDSE construction [42], we pick up the first and the fourth transverse tensor structure such that

$$\Gamma_\mu^f(\tilde{q}, \tilde{p}) = \mathcal{T}_\mu^{f,(1)}(\tilde{q}, \tilde{p}) \lambda^{(1)}(\tilde{q}, \tilde{p}) + \mathcal{T}_\mu^{f,(4)}(\tilde{q}, \tilde{p}) \lambda^{f,(4)}(\tilde{q}, \tilde{p}), \quad (5)$$

with

$$\begin{aligned} \mathcal{T}_\mu^{(1)}(\tilde{q}, \tilde{p}) &= -i\gamma_\mu, \quad \mathcal{T}_\mu^{(4)}(\tilde{q}, \tilde{p}) = i\sigma_{\mu\nu} k_\nu, \\ \sigma_{\mu\nu} &= \frac{i}{2} [\gamma_\mu, \gamma_\nu]. \end{aligned} \quad (6)$$

In the vertex structure, the Dirac structure $\mathcal{T}_\mu^{(1)}$ is the tree level structure and is naturally dominant. The Pauli term $\mathcal{T}_\mu^{(4)}$ is important in the perturbative calculation, and is found to be also dominant in the nonperturbative calculations [43, 44]. Now with the parameterization given in Eq. (1), the dressing function of the Dirac term is given by

$$\lambda^{f,(1)}(\tilde{q}, \tilde{p}) = g_s F(k^2) \left[\delta_{\mu 4} \Sigma_{C^f}(\tilde{q}, \tilde{p}) + (1 - \delta_{\mu 4}) \Sigma_{A^f}(\tilde{q}, \tilde{p}) \right] \quad (7)$$

to satisfy the Slavnov-Taylor identity (STI) for the quark-gluon vertex, where $F(k^2) = k^2 G_c(k)$ denotes the ghost dressing function, and $G_c(k) \delta^{ab}$ is the ghost propagator.

Also, we employ

$$\lambda^{f,(4)}(\tilde{q}, \tilde{p}) = g_s Z_A^{-\frac{1}{2}}(k) \Delta_{B^f}(\tilde{q}, \tilde{p}) \quad (8)$$

following the construction in Eq. [42]. The functions Σ_X and Δ_X are defined as

$$\begin{aligned} \Sigma_X(\tilde{q}, \tilde{p}) &\equiv \frac{X(\tilde{q}) + X(\tilde{p})}{2}, \\ \Delta_X(\tilde{q}, \tilde{p}) &\equiv \frac{X(\tilde{p}) - X(\tilde{q})}{\tilde{p}^2 - \tilde{q}^2}, \end{aligned} \quad (9)$$

with $X(\tilde{p})$ is an arbitrary function of the fermionic momentum argument \tilde{p} .

The information of the ghost dressing function $F(k^2)$ is also needed to evaluate the vertex dressing function (7). In the current work, we take the quantitative result from another functional approach as the input to the ghost dressing function at vacuum, and drop the temperature and baryon chemical potential dependence as an approximation, which is shown to be a milder influence on the current result. The fit function of the ghost dressing function is given by

$$F(k^2) = \frac{a_1 + b_1 \sqrt{k^2} + c_1 k^2}{1 + d_1 \sqrt{k^2} + e_1 k^2}, \quad (10)$$

where the values of the parameters are chosen as [45]

$$\begin{aligned} a_1 &= 3.169 \text{ GeV}^2, & b_1 &= 4.744 \text{ GeV}, & c_1 &= 6.045, \\ d_1 &= 1.558 \text{ GeV}^2, & e_1 &= 6.385 \text{ GeV}. \end{aligned} \quad (11)$$

This then closes the quark gap equation, and the quark propagator can be obtained after putting in the gluon propagator.

B. The gluon gap equation

For the gluon gap equation, we take the following difference form of DSE [32, 42]

$$D_{\mu\nu, \mathbf{v}}^{-1}(k) = D_{\mu\nu, \mathbf{v}_0}^{-1}(k) + \Delta \Pi_{A, \mu\nu}^{\mathbf{v}, \mathbf{v}_0}(k), \quad (12)$$

and here the difference is for the inclusion of the charm quark, which then reads:

$$\begin{aligned} \mathbf{v}_0 &= (N_f = 2 + 1, m_f = (m_l, m_l, m_s), T, \mu_q), \\ \mathbf{v} &= (N_f = 2 + 1 + 1, m_f = (m_l, m_l, m_s, m_c), T, \mu_q). \end{aligned} \quad (13)$$

For the gluon propagator with $2 + 1$ flavor structure $D_{\mu\nu, \mathbf{v}_0}(k) = Z_{A, \mathbf{v}_0}(k)/k^2 \cdot \Pi_{\mu\nu}^\perp$, we use the hard thermal loop approximation to approach the quantitative result, which reads

$$Z_{A, \mathbf{v}_0}(k) = Z_{T, \mu_q}^{\text{trans}}(k), \quad (14)$$

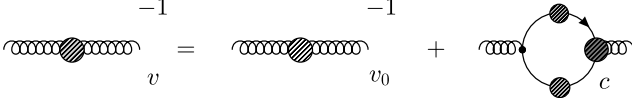


FIG. 1. Feynman diagrams of the difference DSE (12). The black-solid lines with gray-hatched blobs represent the charm quark propagators, and the spiraling lines with gray- or white-hatched blobs denote the gluon propagator in 2+1 or 2+1+1 flavors.

where the right-hand side denotes the transverse gluon propagator dressing at finite temperature and quark chemical potential, and

$$Z_{T,\mu_q}^{\text{trans}}(k) = Z_{\text{vac}}(p) + \frac{2\pi}{3} \alpha_S^{\text{HTL}} \left(T^2 + \frac{\mu_B^2}{3\pi^2} \right) \frac{1}{k^2}, \quad (15)$$

where $\alpha_S^{\text{HTL}} = 0.115$ is the gauge coupling for evaluating the hard thermal loop (HTL) mass. In Eq. (15), we only take into account the light quark loop contribution to the gluon thermal mass, and the strange flavor contribution is dropped due to its heaviness. For the vacuum gluon dressing $Z_{\text{vac}}^{-1}(p)$, we take the following propagator form [42, 44]

$$Z_{\text{vac}}^{-1}(k^2) = \frac{k^2 \frac{a^2 + k^2}{b^2 + k^2}}{M_G^2(k^2) + k^2 [1 + c \log(d^2 k^2 + e^2 M_G^2(k^2))]^\gamma}, \quad (16)$$

in which

$$M_G^2(k^2) = \frac{f^4}{g^2 + k^2}, \quad (17)$$

and $\gamma = \frac{13 - \frac{4}{3} N_f}{22 - \frac{4}{3} N_f}$ is the perturbative anomalous dimension of the gluon propagator. Here we choose $N_f = 3$ to match the (2+1)-flavor result of the gluon propagator. The values of the parameters are chosen as

$$\begin{aligned} a &= 1 \text{ GeV}, & b &= 0.735 \text{ GeV}, & c &= 0.12, \\ d &= 0.0257 \text{ GeV}^{-1}, & e &= 0.081 \text{ GeV}^{-1}. \end{aligned} \quad (18)$$

in the gluon propagator (16) and

$$f = 0.65 \text{ GeV}, \quad g = 0.87 \text{ GeV}, \quad (19)$$

in the gluon mass (17), to fit with the (2+1)-flavor data from the functional approaches [44].

The self-energy in the difference DSE (12) for the gluon propagator is then given by the charm quark vacuum polarization

$$\begin{aligned} \Delta \Pi_{A,\mu\nu}^{\mathbf{v},\mathbf{v}_0}(k) &= -\frac{Z_1^f}{2} g_s^{\text{HTL}} \int_q \text{tr} \left[\gamma_\mu S^c(\tilde{q}) \Gamma_\nu^c(\tilde{q}, \tilde{q} - k) S^c(\tilde{q} - k) \right]. \end{aligned} \quad (20)$$

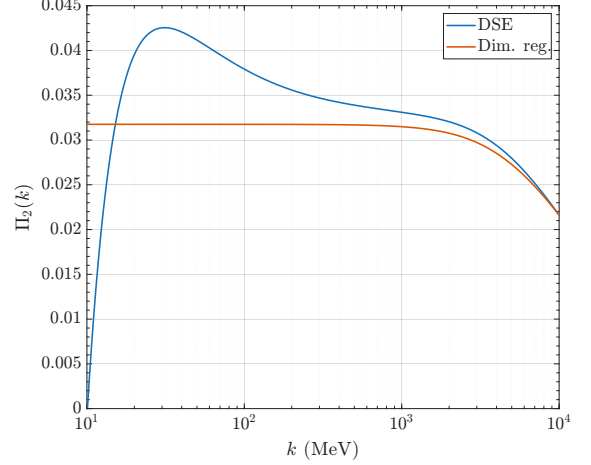


FIG. 2. Dimensionless gluon self-energies $\Pi_2(k)$ evaluated from the DSE (20) (blue-solid line) and the dim. reg. (24) (Orange-solid line) at the vacuum.

which is diagrammatically shown in Fig. 1, and $g_s^{\text{HTL}} = \sqrt{4\pi\alpha_s^{\text{HTL}}}$. The tensor structure $\mathcal{T}_\nu^{(4)}$ has been found to be negligible in the gluon self energy [42, 46], and hence here for simplicity, we only keep the Dirac term in the evaluation of Eq. (20).

Note that there exists quadratic divergence in Eq. (20), which in the perturbative calculation, requires the dimensional regularization. For the nonperturbative calculation, we perform the Brown-Pennington projection procedure to separate the divergence induced by the ultraviolet (UV) cutoff Λ from the temperature T in the quark loop integral [47, 48]. The projection for the self-energy is defined as:

$$\Pi_{\mu\nu}^{\text{B-P}} = \delta_{\mu\nu} - 4 \frac{k_\mu k_\nu}{k^2}. \quad (21)$$

The dimensionless gluon self-energy $\Pi_2(k)$ is obtained from the projection as

$$\Pi_2(k) = \frac{\Delta \Pi_{A,\mu\nu}^{\mathbf{v},\mathbf{v}_0}(k) \Pi_{\mu\nu}^{\text{B-P}}(k)}{3k^2}. \quad (22)$$

The quadratic divergence in the self-energy can be subtracted after this projection, and only the logarithmic divergence is left which is absorbed by the renormalization constant. In comparison, we also present the benchmark result from the vacuum charm quark loop with the bare vertex and the tree-level-like propagator based on the dimensional regularization (dim. reg.), that

$$\Delta \Pi_{A,\mu\nu}^{\mathbf{v},\mathbf{v}_0}(k) = \Pi_{\mu\nu}^\perp \cdot \Pi_{2,\text{vac}}(k) k^2, \quad (23)$$

where the scalar part of the gluon self-energy reads [49]

$$\begin{aligned} \Pi_{2,\text{vac}}(k, \mu) &= \frac{\alpha_s(\mu)}{\pi} \int_0^1 dx x(1-x) \log \left[\frac{(m_c^2 + \mu^2 x(1-x))}{(m_c^2 + k^2 x(1-x))} \right], \end{aligned} \quad (24)$$

where m_c is the current quark mass of the charm quark. In Fig. 2, we show the dimensionless gluon self-energies $\Pi_2(k)$ from Eq. (20) by solving the coupled DSEs at the vacuum, and the one from Eq. (24). Both agree with each other in the UV region down to the momentum scale around $k \sim 1$ GeV. In the IR region, the full quark propagator and quark gluon vertex lead to an enhancement in the self-energy of the gluon propagator.

III. RESULTS

The impact of the charm quark on the QCD phase transition, is mainly determined by the quark gap equation. Therefore, the charm quark effect is validated through the quark anti-quark self-energy loop in the gluon propagator as in Eq. 12. The setup in the previous section is thus complete for studying the charm quark effect, and in this section we present the numerical results.

A. The consistency check in vacuum

The above-described scheme for DSEs has enabled one to obtain the quark and gluon propagator. The parameters required to solve the equations are only the coupling constant and the current quark masses, which can be determined by the physical quantities. After determining these parameters, we then compare the results for 2+1 and 2+1+1 flavors in vacuum.

At vanishing temperature, the quark inverse-propagator can be simply parameterized in $O(4)$ symmetric form as

$$[S^f(p^2)]^{-1} = i\not{p}A^f(p^2) + B^f(p^2), \quad (25)$$

from which we can read off the quark mass functions as $M_f(p^2) = B^f(p^2)/A^f(p^2)$, and the quark wave-function is $Z_f(p^2) = A^f(p^2)$. The quark condensate can be calculated by

$$\langle \bar{\psi}\psi \rangle = 4N_c \int_p \frac{m_l M_l^r}{Z_l(p^2 + M_l^2)}, \quad (26)$$

with $M_l^r(p^2) = M(p^2) - m_l \partial_{m_l} M(p^2)$. For the 2+1 flavor case, we take the coupling constant as $\alpha_s = 0.257$, and get

$$\langle \bar{\psi}\psi \rangle^{\frac{1}{3}} = 372.7 \text{ MeV}, \quad m_l = 1.8 \text{ MeV}, \quad \frac{m_s}{m_l} = 27, \quad (27)$$

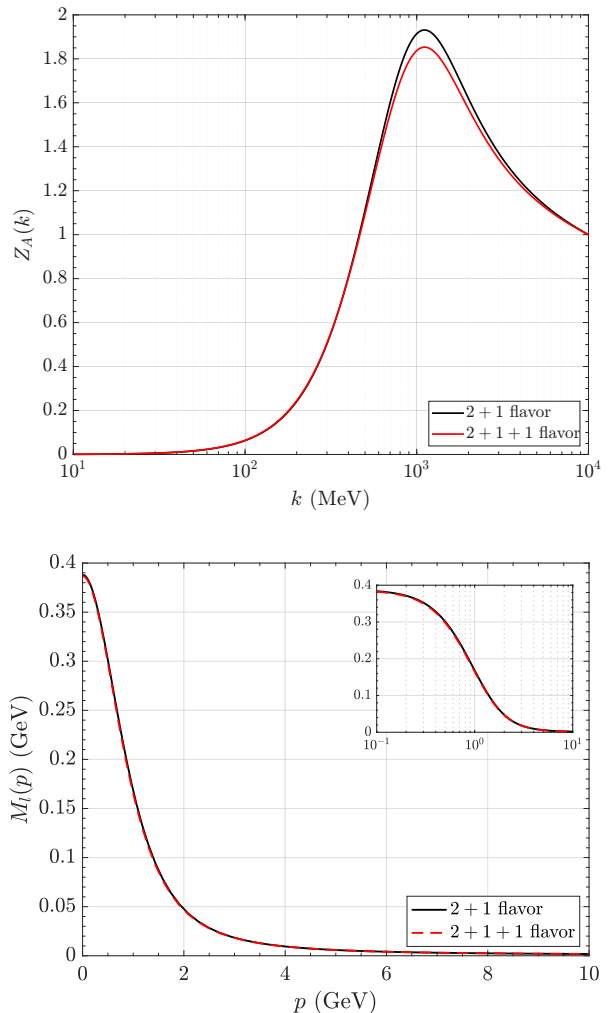


FIG. 3. Top panel: the dressing function $Z_A(k)$ of the gluon propagator in the 2 + 1 flavor case (black-solid line), and in the 2 + 1 + 1 flavor case with charm loop evaluated from DSE (red-solid line). Bottom panel: the mass function $M_l(p)$ of the light quark flavors in the 2+1 flavor case (blue-solid line), and in the 2 + 1 + 1 flavor case with charm loop from DSE (orange-dashed line). These results are obtained by solving the coupled DSEs in the vacuum.

at the renormalization scale $\mu = 10$ GeV. The current quark mass of light quarks is chosen to satisfy the Gell-Mann–Oakes–Renner (GMOR) relation with the empirical values of the pion mass $m_\pi = 135$ MeV where the pion decay constant f_π is evaluated through the Pagels–Stokar (PS) formula [32]

$$f_\pi = \frac{4N_c}{N_\pi} \int_p \frac{M_l^r}{Z_l(p^2 + M_l^2)} \left[M_l - \frac{p^2}{2} \frac{\partial M_l}{\partial p^2} \right], \quad (28)$$

with the normalization factor N_π of the Bethe-Salpeter

wave function of the pion obtained by solving

$$N_\pi^2 = f_\pi N_\pi + 2N_c \int_p \frac{(M_l^T)^2 (p^2 Z_l Z_l'' + 2Z_l Z_l' - p^2 Z_l'')}{Z_l^2 (p^2 + M_l^2)}, \quad (29)$$

where $Z_l'(p^2) = \partial_{p^2} Z_l(p^2)$, $Z_l''(p^2) = \partial_{p^2}^2 Z_l(p^2)$. With the PS formula, we get $f_\pi = 101.1$ MeV, which is consistent with the previous calculation within the PS formal [44].

For the $2 + 1 + 1$ flavor case, we put the following parameters as:

$$\alpha_s = 0.255, \quad m_l = 1.8 \text{ MeV}, \quad \frac{m_s}{m_l} = 27, \\ m_c = 1270 \text{ MeV}, \quad (30)$$

More importantly, we depict the mass function of the light quarks and the dressing function of the gluon propagator obtained in vacuum as in Fig. 3. First of all, as shown in the lower panel of Fig. 3, the light quark mass functions, after calibrating the parameters with pion mass and decay constants, are consistent in $2+1$ and $2+1+1$ cases. Due to the additional charm quark loop, the gluon propagator is suppressed. The peak height of the gluon dressing function $Z_A(k)$ is modified from 1.93 in the $2+1$ flavor into 1.85 in the $2+1+1$ flavor. Nevertheless, the mass scale of the gluon propagator, i.e., the location of the maximum point in the dressing function, is barely changed. Besides, the charm quark loop gradually decouples from the UV running behavior, which is revealed as the dressing function in two cases, and gradually converges at around $k \sim 10$ GeV.

B. QCD chiral phase diagram at $N_f = 2 + 1 + 1$

	$T_c(\mu_B = 0)$ (MeV)	$(T^{\text{CEP}}, \mu_B^{\text{CEP}})$ (MeV)
miniDSE [42]	156.5	(108.5, 567)
fRG [35]	156	(107, 635)
fRG-DSE: STI construction [32]	154	(93, 672)
fRG-DSE: self-consistent [33]	155	(109, 610)
DSE [34]	157	(117, 600)
This work: $2 + 1$ flavor	152.3	(102.9, 618.8)
This work: $2 + 1 + 1$ flavor	151.0	(104.3, 600.1)

TABLE I. The impact of charm quark loop of the CEP location of the chiral phase diagrams together with the results of $N_f = 2 + 1$ in Refs. [32–35, 42]. Note that here we apply the HTL gluon mass to incorporate the light quark effects in the gluon propagator, which is similar to the approximation applied in Ref. [11].

By scanning the chiral condensate in the temperature and chemical potential plane, we obtain the chiral phase diagram for $N_f = 2 + 1$ and $N_f = 2 + 1 + 1$. In Fig. 4, we show our results together with the previous studies from functional QCD methods. First of all, the inclusion

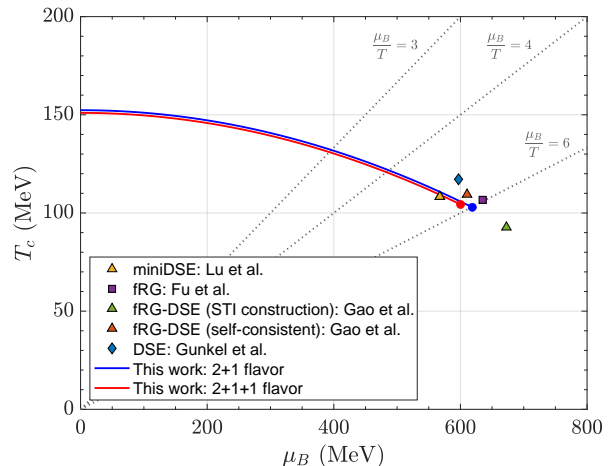


FIG. 4. QCD chiral phase diagram obtained within the current framework (solid lines) with benchmark results of the critical end point (colored marks). The benchmark results come from the Ref. [42] with the miniDSE scheme (yellow triangle), the fRG method [35], the fRG-DSE scheme with STI construction [32] (green triangle) and with the self-consistent setup [33] (orange triangle), and from the DSE method [34]. The solid lines correspond to the cases of the $2+1$ flavor (blue line) and the $2+1+1$ flavor with the DSE charm loop (20) (red line).

of the charm quark loop does not have an impact on the curvature of the phase transition line. The phase transition line of $N_f = 2 + 1 + 1$ gets along with the line of $N_f = 2 + 1$ in the whole crossover region. The effect of the charm quark loop on the chiral phase transition is mainly on the location of CEP, that is, the inclusion of the charm quark loop makes the CEP appear at a lower chemical potential. Note that the effect essentially comes from the difference of the mass scale in the gluon propagator as depicted in Fig. 3. A larger mass scale with the inclusion of charm quark loop gives a lower peak at intermediate momentum in the dressing and consequently a more rapid declining in the gluon propagator, which leads to an earlier CEP.

Furthermore, we list the values for the CEP location in Tab. I in comparison to the previous studies. After including the charm quark loop, the location of the CEP deviates from the one obtained in the $2+1$ flavor case by a size of around 1.4% in temperature and around 3.0% in the baryon chemical potential. As has been discussed widely in the previous studies in functional QCD approaches, the up-to-date truncation scheme in functional approaches has made it possible to deliver a converging estimate on the CEP location, which is predicted to be in the ballpark around $\mu_B \sim 600$ MeV. It is certainly of great importance to check the impact of the higher order correlations in the gap equation, for instance, the hadron resonance channel in the quark gluon vertex, the heavy quark loop in the gluon propagator, and also the combination of the Polyakov loop in the gap equation. In

particular, these higher-order correlations open an access for the precision calculations for larger chemical potential $\mu_B/T > 4$. Nevertheless, as illustrated here and also the works in Ref. [29, 34], the impact of these correlations leads to around 3% deviations.

IV. SUMMARY

In this work, we have investigated the impact of charm quark fluctuations on the chiral phase structure of QCD. Motivated by recent theoretical and experimental developments suggesting that heavy quarks may provide a non-negligible influence on the IR properties of QCD matter, we conducted a comparative analysis between the conventional $2 + 1$ flavor setup and an extended $2 + 1 + 1$ flavor system that includes the dynamical charm quark.

To achieve a controlled and computationally efficient analysis, we employed the recently proposed miniDSE approach, a numerically optimized truncation scheme of the DSEs. This framework allows for the consistent treatment of different quark flavors while preserving essential nonperturbative features such as dynamical chiral symmetry breaking. Within this setup, we solved the truncated gap equations at finite temperature and baryon chemical potential for both flavor configurations, ensuring all model parameters and renormalization conditions were fixed in the vacuum to allow for direct, self-consistent comparison.

Our results demonstrate that the inclusion of the charm quark induces a noticeable modification in the chiral phase diagram. In particular, we observe a sizable change in the location of the CEP when comparing the $2 + 1$ and $2 + 1 + 1$ cases. Additionally, the crossover boundary of the chiral transition also shows subtle but

non-negligible modifications in its curvature and extent. These effects are especially relevant given the growing interest in the precise determination of the QCD phase diagram from both theoretical predictions and experimental programs at RHIC, LHC, and future facilities.

We interpret this shift in the phase structure as a manifestation of the charm quark's indirect yet tangible contribution to the chiral dynamics of QCD. While heavy quarks are commonly assumed to decouple from low-energy phenomena due to their large masses, our findings suggest that their influence, although moderate, cannot be entirely neglected, particularly when aiming for precision descriptions of QCD thermodynamics and critical behavior. This observation may also extend to the bottom quark, whose contributions, though smaller due to its even larger mass, could become relevant under extreme conditions such as those realized in heavy-ion collisions or the interiors of compact stars.

In summary, our analysis highlights the importance of incorporating heavy-flavor effects in studies of the QCD phase structure, especially in the context of high-precision non-perturbative modeling. The subtle but systematic modifications introduced by charm quark dynamics underscore the need to go beyond the traditional light-flavor perspective when exploring the critical phenomena and thermodynamic properties of strongly interacting matter.

ACKNOWLEDGMENTS

The work of F. G. is supported by the National Science Foundation of China (NSFC) under Grant No. 12305134. The work of S. M. is supported by the NSFC under Grant No. 11747308, 11975108, 12047569, and the Seeds Funding of Jilin University (S.M.).

-
- [1] M. M. Aggarwal *et al.* (STAR), (2010), [arXiv:1007.2613 \[nucl-ex\]](#).
 - [2] B. Mohanty (STAR), *J. Phys. G* **38**, 124023 (2011), [arXiv:1106.5902 \[nucl-ex\]](#).
 - [3] X. Luo and N. Xu, *Nucl. Sci. Tech.* **28**, 112 (2017), [arXiv:1701.02105 \[nucl-ex\]](#).
 - [4] T. Nonaka, *JPS Conf. Proc.* **26**, 024007 (2019).
 - [5] J. Chen *et al.*, *Nucl. Sci. Tech.* **35**, 214 (2024), [arXiv:2407.02935 \[nucl-ex\]](#).
 - [6] M. Buballa, *Phys. Rept.* **407**, 205 (2005), [arXiv:hep-ph/0402234](#).
 - [7] K. Fukushima and C. Sasaki, *Prog. Part. Nucl. Phys.* **72**, 99 (2013), [arXiv:1301.6377 \[hep-ph\]](#).
 - [8] M. Oertel, M. Hempel, T. Klähn, and S. Typel, *Rev. Mod. Phys.* **89**, 015007 (2017), [arXiv:1610.03361 \[astro-ph.HE\]](#).
 - [9] N. Aghanim *et al.* (Planck), *Astron. Astrophys.* **641**, A6 (2020), [Erratum: *Astron. Astrophys.* 652, C4 (2021)], [arXiv:1807.06209 \[astro-ph.CO\]](#).
 - [10] F. Gao and I. M. Oldengott, *Phys. Rev. Lett.* **128**, 131301 (2022), [arXiv:2106.11991 \[hep-ph\]](#).
 - [11] H.-w. Zheng, F. Gao, L. Bian, S.-x. Qin, and Y.-x. Liu, *Phys. Rev. D* **111**, L021303 (2025), [arXiv:2407.03795 \[hep-ph\]](#).
 - [12] F. Gao, J. Harz, C. Hati, Y. Lu, I. M. Oldengott, and G. White, *JHEP* **06**, 247 (2025), [arXiv:2407.17549 \[hep-ph\]](#).
 - [13] G. Y. Shao, M. Di Toro, V. Greco, M. Colonna, S. Plumari, B. Liu, and Y. X. Liu, *Phys. Rev. D* **84**, 034028 (2011), [arXiv:1105.4528 \[nucl-th\]](#).
 - [14] X. Y. Xin, S. X. Qin, and Y. X. Liu, *Phys. Rev. D* **90**, 076006 (2014), [arXiv:2109.09935 \[hep-ph\]](#).
 - [15] S. He, S.-Y. Wu, Y. Yang, and P.-H. Yuan, *JHEP* **04**, 093 (2013), [arXiv:1301.0385 \[hep-th\]](#).
 - [16] K. Chelabi, Z. Fang, M. Huang, D. Li, and Y.-L. Wu, *JHEP* **04**, 036 (2016), [arXiv:1512.06493 \[hep-ph\]](#).
 - [17] T. Kojo, D. Hou, J. Okafor, and H. Togashi, *Phys. Rev. D* **104**, 063036 (2021), [arXiv:2012.01650 \[astro-ph.HE\]](#).
 - [18] X. Chen, L. Zhang, D. Li, D. Hou, and M. Huang, *JHEP* **07**, 132 (2021), [arXiv:2010.14478 \[hep-ph\]](#).

- [19] M. Hippert, J. Grefa, T. A. Manning, J. Noronha, J. Noronha-Hostler, I. Portillo Vazquez, C. Ratti, R. Rougemont, and M. Trujillo, (2023), [arXiv:2309.00579 \[nucl-th\]](#).
- [20] R. G. Cai, S. He, L. Li, and Y. X. Wang, *Phys. Rev. D* **106**, L121902 (2022), [arXiv:2201.02004 \[hep-th\]](#).
- [21] X. Chen, D. Li, and M. Huang, *Chin. Phys. C* **43**, 023105 (2019), [arXiv:1810.02136 \[hep-ph\]](#).
- [22] G. Basar, *Phys. Rev. C* **110**, 015203 (2024), [arXiv:2312.06952 \[hep-th\]](#).
- [23] A. Adam, S. Borsányi, Z. Fodor, J. N. Guenther, P. Parotto, A. Pásztor, D. Pesznyák, L. Pirelli, and C. H. Wong, *PoS LATTICE2024*, 178 (2025), [arXiv:2502.03211 \[hep-lat\]](#).
- [24] C. Ecker, N. Jokela, and M. Järvinen, (2025), [arXiv:2506.10065 \[astro-ph.HE\]](#).
- [25] S. Borsanyi, Z. Fodor, J. N. Guenther, R. Kara, S. D. Katz, P. Parotto, A. Pásztor, C. Ratti, and K. K. Szabo, *Phys. Rev. Lett.* **125**, 052001 (2020), [arXiv:2002.02821 \[hep-lat\]](#).
- [26] A. Bazavov *et al.* (HotQCD), *Phys. Lett. B* **795**, 15 (2019), [arXiv:1812.08235 \[hep-lat\]](#).
- [27] C. Bonati, M. D’Elia, F. Negro, F. Sanfilippo, and K. Zambello, *Phys. Rev. D* **98**, 054510 (2018), [arXiv:1805.02960 \[hep-lat\]](#).
- [28] S. X. Qin, L. Chang, H. Chen, Y. X. Liu, and C. D. Roberts, *Phys. Rev. Lett.* **106**, 172301 (2011), [arXiv:1011.2876 \[nucl-th\]](#).
- [29] C. S. Fischer, J. Luecker, and C. A. Welzbacher, *Phys. Rev. D* **90**, 034022 (2014), [arXiv:1405.4762 \[hep-ph\]](#).
- [30] F. Gao and Y. X. Liu, *Phys. Rev. D* **94**, 076009 (2016), [arXiv:1607.01675 \[hep-ph\]](#).
- [31] C. S. Fischer, *Prog. Part. Nucl. Phys.* **105**, 1 (2019), [arXiv:1810.12938 \[hep-ph\]](#).
- [32] F. Gao and J. M. Pawłowski, *Phys. Rev. D* **102**, 034027 (2020), [arXiv:2002.07500 \[hep-ph\]](#).
- [33] F. Gao and J. M. Pawłowski, *Phys. Lett. B* **820**, 136584 (2021), [arXiv:2010.13705 \[hep-ph\]](#).
- [34] P. J. Gunkel and C. S. Fischer, *Phys. Rev. D* **104**, 054022 (2021), [arXiv:2106.08356 \[hep-ph\]](#).
- [35] W. J. Fu, J. M. Pawłowski, and F. Rennecke, *Phys. Rev. D* **101**, 054032 (2020), [arXiv:1909.02991 \[hep-ph\]](#).
- [36] N. Dupuis, L. Canet, A. Eichhorn, W. Metzner, J. M. Pawłowski, M. Tissier, and N. Wschebor, *Phys. Rept.* **910**, 1 (2021), [arXiv:2006.04853 \[cond-mat.stat-mech\]](#).
- [37] W. J. Fu, *Commun. Theor. Phys.* **74**, 097304 (2022), [arXiv:2205.00468 \[hep-ph\]](#).
- [38] B. E. Aboona *et al.* (STAR), *Phys. Rev. Lett.* **135**, 142301 (2025), [arXiv:2504.00817 \[nucl-ex\]](#).
- [39] H. van Hees, V. Greco, and R. Rapp, *Phys. Rev. C* **73**, 034913 (2006), [arXiv:nucl-th/0508055](#).
- [40] K. Goswami, K. K. Pradhan, D. Sahu, J. Dey, and R. Sahoo, *Phys. Rev. D* **111**, 014029 (2025), [arXiv:2409.13255 \[hep-ph\]](#).
- [41] C. A. Welzbacher, C. S. Fischer, and J. Luecker, *J. Phys. Conf. Ser.* **599**, 012015 (2015), [arXiv:1412.3650 \[hep-ph\]](#).
- [42] Y. Lu, F. Gao, Y.-X. Liu, and J. M. Pawłowski, *Phys. Rev. D* **110**, 014036 (2024), [arXiv:2310.18383 \[hep-ph\]](#).
- [43] C. Tang, F. Gao, and Y.-X. Liu, *Phys. Rev. D* **100**, 056001 (2019), [arXiv:1902.01679 \[hep-ph\]](#).
- [44] F. Gao, J. Papavassiliou, and J. M. Pawłowski, *Phys. Rev. D* **103**, 094013 (2021), [arXiv:2102.13053 \[hep-ph\]](#).
- [45] A. C. Aguilar, C. O. Ambrósio, F. De Soto, M. N. Ferreira, B. M. Oliveira, J. Papavassiliou, and J. Rodríguez-Quintero, *Phys. Rev. D* **104**, 054028 (2021), [arXiv:2107.00768 \[hep-ph\]](#).
- [46] Y. Lu, F. Gao, Y.-x. Liu, and J. M. Pawłowski, (2025), [arXiv:2504.05099 \[hep-ph\]](#).
- [47] N. Brown and M. R. Pennington, *Phys. Rev. D* **38**, 2266 (1988).
- [48] C. S. Fischer and J. Luecker, *Phys. Lett. B* **718**, 1036 (2013), [arXiv:1206.5191 \[hep-ph\]](#).
- [49] M. D. Schwartz, *Quantum Field Theory and the Standard Model* (Cambridge University Press, 2014).